Eur. Phys. J. Spec. Top.
https://doi.org/10.1140/epjs/s11734-022-00669-5

THE EUROPEAN PHYSICAL JOURNAL SPECIAL TOPICS

Regular Article

Spin effects in ultrafast laser-plasma interactions

Giovanni Manfredi[1,a], Paul-Antoine Hervieux[1], and Nicolas Crouseilles[2]

[1] Institut de Physique et Chimie des Matériaux de Strasbourg, UMR 7504, Université de Strasbourg, CNRS, 67000 Strasbourg, France
[2] Inria Rennes Bretagne Atlantique (Mingus) and IRMAR UMR CNRS 6625, Université de Rennes, 35042 Rennes, France

Received 15 May 2022 / Accepted 20 September 2022

Abstract Ultrafast laser pulses interacting with plasmas can give rise to a rich spectrum of physical phenomena, which have been extensively studied both theoretically and experimentally. Less work has been devoted to the study of polarized plasmas, where the electron spin may play an important role. In this short review, we illustrate the use of phase-space methods to model and simulate spin-polarized plasmas. This approach is based on the Wigner representation of quantum mechanics, and its classical counterpart, the Vlasov equation, which are generalized to include the spin degrees of freedom. Our approach is illustrated through the study of the stimulated Raman scattering of a circularly polarized electromagnetic wave interacting with a dense electron plasma.

1 Introduction

Laser-matter interactions have a long history in many areas of physics. In condensed-matter and nanophysics, laser pulses are used to investigate the electron response on ultrafast time scales— femtosecond and, more recently, attosecond. Indeed, the most typical electronic resonance for conduction electrons in metals (i.e., the plasmon resonance) lies in the femtosecond range, so that ultrafast laser pulses constitute an invaluable experimental tool to probe the collective electron response [1, 2]. Among the many possible applications, plasmonic resonances are routinely investigated in biomedicine [3, 4] and high-harmonic generation [5–7].

Laser–plasma interactions also play an important role in plasma physics, particularly inertial fusion [8] and laser–plasma accelerators [9, 10]. The latter are based on the acceleration of charged particles by large-amplitude plasma waves, which can be generated, among others, through the stimulated Raman scattering mechanism [11–13] discussed in the present work.

However, electrons possess not only an electric charge, but also a spin, i.e. an intrinsic magnetic moment. The use of the electron spin to store and transfer information is at the basis of the currently burgeoning field of spintronics [14, 15].

In nanophysics, spin effects are epitomized by the unexpected loss of magnetization occurring on the femtosecond timescale after irradiation of a ferromagnetic thin film with a laser pulse [2, 16]. This effect was variously attributed to mechanisms such as the spin-orbit interaction [17, 18] or the superdiffusive electron transport induced by the electromagnetic field [19], although it has never been fully elucidated.

In plasma physics, the study of spin-dependent effects is much more recent. However, polarized electron beams of high spin polarization can now be created and precisely manipulated in the laboratory [20–22]. Theoretical work on polarized plasmas dates back from the 1980s [23], and was much revived during the last decade [7, 24–27]. Recently, Brodin et al. [28] developed a particle-in-cell (PIC) code that includes the magnetic dipole force and magnetization currents associated with the electron spin. PIC methods for particles with spin were also developed for applications to laser–plasma interactions [29].

Most existing works on the spin dynamics in the condensed-matter and nanophysics communities rely on wavefunction-based methods, notably the time-dependent density functional theory (TD-DFT) extended to include spin effects [17, 30–32]. Here, we propose a different approach based on Wigner functions. In the Wigner representation, quantum states are represented by a function of the phase-space variables plus time, which evolves according to an integrodifferential equation (Wigner equation). The classical limit of the Wigner equation coincides with the

Communicated by Guest editors: Franck Lépine, Lionel Poisson.

Ultrafast Phenomena from attosecond to picosecond timescales: theory and experiments.

[a] e-mail: giovanni.manfredi@ipcms.unistra.fr (corresponding author)

Vlasov equation, well-known from plasma physics to describe the dynamics of a collisionless plasma in the mean-field approximation. Recently, this phase-space approach was extended to systems with spin-dependent degrees of freedom. More details on the foundations of these methods can be found in our recent review [33].

2 Phase-space dynamics with spin

For a particle without spin, the Wigner function is a scalar that depends on the phase-space variables and time: $f(\boldsymbol{r},\boldsymbol{v},t)$. It can be used as a classical probability density to compute mean values, e.g.:

$$\langle \boldsymbol{r} \rangle = \frac{\int\int \boldsymbol{r} f(\boldsymbol{r},\boldsymbol{v},t) d\boldsymbol{r} d\boldsymbol{v}}{\int\int f(\boldsymbol{r},\boldsymbol{v},t) d\boldsymbol{r} d\boldsymbol{v}}.$$

However, it is not a true probability density, as it can take negative values.

To extend the Wigner formalism to particles endowed with spin degrees of freedom, two approaches are possible, which we describe in the forthcoming paragraphs.

2.1 Matrix approach

For spin-1/2 particles such as electrons, the Wigner function becomes a 2×2 matrix [34]:

$$\mathcal{F} = \begin{pmatrix} f^{\uparrow\uparrow} & f^{\uparrow\downarrow} \\ f^{\downarrow\uparrow} & f^{\downarrow\downarrow} \end{pmatrix}, \tag{1}$$

where $\uparrow,\downarrow$ denote respectively the spin-up and spin-down components. By projecting the matrix $\mathcal{F}$ onto the Pauli basis set [35], we can write

$$\mathcal{F} = \frac{1}{2}\sigma_0 f_0 + \frac{1}{2}\boldsymbol{f}\cdot\boldsymbol{\sigma}, \tag{2}$$

where

$$f_0 = \mathrm{Tr}\{\mathcal{F}\} = f^{\uparrow\uparrow} + f^{\downarrow\downarrow}, \qquad \boldsymbol{f} = \mathrm{Tr}(\mathcal{F}\boldsymbol{\sigma}), \tag{3}$$

$\boldsymbol{f} = (f_x, f_y, f_z)$, and $\boldsymbol{\sigma} = (\sigma_x, \sigma_y, \sigma_z)$ are the Pauli matrices.

The quantum and semiclassical dynamics of the distribution functions f_0 and $\boldsymbol{f}$ were derived in [7, 24]. Taking the classical limit in the orbital variables, but retaining the quantum nature of the spin, one obtains the following system of equations:

$$\begin{aligned}
&\frac{\partial f_0}{\partial t} + \boldsymbol{v}\cdot\boldsymbol{\nabla} f_0 - \frac{e}{m}(\boldsymbol{E}+\boldsymbol{v}\times\boldsymbol{B})\cdot\boldsymbol{\nabla}_v f_0 \\
&\quad + \frac{\mu_B}{2mc^2}(\boldsymbol{E}\times\boldsymbol{\nabla})_i f_i - \frac{\mu_B}{m}\boldsymbol{\nabla}\left[B_i - \frac{1}{2c^2}(\boldsymbol{v}\times\boldsymbol{E})_i\right]\cdot\boldsymbol{\nabla}_v f_i \\
&\quad - \frac{\mu_B e}{2m^2c^2}[\boldsymbol{E}\times(\boldsymbol{B}\times\boldsymbol{\nabla}_v)]_i f_i = 0. \qquad (4) \\
&\frac{\partial f_i}{\partial t} + \boldsymbol{v}\cdot\boldsymbol{\nabla} f_i - \frac{e}{m}(\boldsymbol{E}+\boldsymbol{v}\times\boldsymbol{B})\cdot\boldsymbol{\nabla}_v f_i \\
&\quad + \frac{\mu_B}{2mc^2}(\boldsymbol{E}\times\boldsymbol{\nabla})_i f_0 - \frac{\mu_B}{m}\boldsymbol{\nabla}\left[B_i - \frac{1}{2c^2}(\boldsymbol{v}\times\boldsymbol{E})_i\right] \\
&\quad \cdot\boldsymbol{\nabla}_v f_0 - \frac{\mu_B e}{2m^2c^2}[\boldsymbol{E}\times(\boldsymbol{B}\times\boldsymbol{\nabla}_v)]_i f_0 \\
&\quad - \frac{2\mu_B}{\hbar}\left\{\left[\boldsymbol{B} - \frac{1}{2c^2}(\boldsymbol{v}\times\boldsymbol{E})\right]\times\boldsymbol{f}\right\}_i = 0. \qquad (5)
\end{aligned}$$

where $i = (x,y,z)$, $\mu_B = e\hbar/(2m)$ is the Bohr magneton, c is the speed of light, and $e>0$ and m are respectively the electron charge and mass. The electromagnetic fields $(\boldsymbol{E},\boldsymbol{B})$ can be either external (e.g., a laser pulse) or internal, generated self-consistently by the plasma. In the latter case, they should be computed by solving the corresponding Maxwell equations, see also Sect. 2.2. Note that, in the above "spin-Vlasov" equations, the orbital motion is purely classical, while the spin is treated as a fully quantum variable [7, 24].

In the Eqs. (4)–(5), all the terms preceded by the factor c^{-2} represent the spin-orbit interaction. In the present work such terms will be neglected, but we still write them here for completeness.

Recently, we have used the above matrix approach to study the generation of spin currents in nickel films [36].

2.2 Scalar approach

An alternative, but equivalent, method consists in defining a scalar probability distribution $g(\boldsymbol{r},\boldsymbol{v},\boldsymbol{s},t)$ that evolves in an extended phase space, where the spin $\boldsymbol{s}$ is treated as a classical unit vector [25, 37].

In the semiclassical limit [26], and neglecting the spin-orbit coupling terms, the scalar spin-Vlasov equation reads as:

$$\begin{aligned}
&\frac{\partial g}{\partial t} + \boldsymbol{v}\cdot\nabla g - \left[\frac{e}{m}(\boldsymbol{E}+\boldsymbol{v}\times\boldsymbol{B}) + \frac{\mu_B}{m}\nabla(\boldsymbol{s}\cdot\boldsymbol{B})\right. \\
&\quad \left. + \frac{\mu_B}{m}\nabla\left(\boldsymbol{B}\cdot\frac{\partial}{\partial\boldsymbol{s}}\right)\right]\cdot\frac{\partial g}{\partial\boldsymbol{v}} \\
&\quad - \frac{2\mu_B}{\hbar}\boldsymbol{s}\times\boldsymbol{B}\cdot\frac{\partial g}{\partial\boldsymbol{s}} = 0.
\end{aligned} \tag{6}$$

In the forthcoming simulations, the last term in front of $\partial g/\partial\boldsymbol{v}$ will be neglected. This is also a semiclassical approximation, which can be justified by assuming that variations of g in spin space are of moderate size (for more details, see [25, 38, 39]). It should also be pointed out that this quantum term contains derivatives in both real and spin space, thus making the PIC algorithm much more involved.

For self-consistent problems, the above Vlasov equation should be coupled to the Maxwell equations

$$\begin{aligned} \epsilon_0\mu_0\frac{\partial \boldsymbol{E}}{\partial t} &= \nabla\times\boldsymbol{B}+\mu_0\boldsymbol{J},\\ \frac{\partial \boldsymbol{B}}{\partial t} &= -\nabla\times\boldsymbol{E},\\ \nabla\cdot\boldsymbol{E} &= \frac{\rho_0-\rho}{\epsilon_0},\\ \nabla\cdot\boldsymbol{B} &= 0, \end{aligned} \tag{7}$$

where the electronic charge and current densities are defined as:

$$\rho = e\int g\,d\boldsymbol{v}d\boldsymbol{s},\quad \boldsymbol{J} = e\int \boldsymbol{v}\,g\,d\boldsymbol{v}d\boldsymbol{s}+\mu_B\nabla\times\int \boldsymbol{s}\,g\,d\boldsymbol{v}d\boldsymbol{s}, \tag{8}$$

and $\rho_0(\boldsymbol{r})$ is a fixed positive charge density (jellium approximation), which will be assumed to be uniform in space in the forthcoming simulations. Note the spin contribution in the definition of the current (second term on the right).

The relationship between the matrix Wigner function $\mathcal{F}(\boldsymbol{r},\boldsymbol{v},t)$ and the scalar function $g(\boldsymbol{r},\boldsymbol{v},\boldsymbol{s},t)$ is as follows:

$$g(\boldsymbol{r},\boldsymbol{v},\boldsymbol{s},t) = \frac{1}{4\pi}\sum_{\alpha,\beta=1}^{2}\left(\delta_{\alpha\beta}+\boldsymbol{s}\cdot\boldsymbol{\sigma}_{\alpha\beta}\right)\mathcal{F}_{\beta\alpha}(\boldsymbol{r},\boldsymbol{v},t), \tag{9}$$

where $\delta_{\alpha\beta}$ is the Kronecker delta and $\boldsymbol{\sigma}_{\alpha\beta}$ represents an element of one of the Pauli matrices $\boldsymbol{\sigma}=(\sigma_x,\sigma_y,\sigma_z)$.

The scalar approach will be used in the next section to study the effect of the electron spin on the Raman scattering of an electromagnetic wave in a plasma.

Finally, we mention another scalar method to model the spin dynamics [40]. In this method, the distribution function only depends on the standard phase-space variables $(\boldsymbol{r},\boldsymbol{v})$, but is supplemented by a second phase-space distribution for the spins, also dependent on $(\boldsymbol{r},\boldsymbol{v})$.

3 Stimulated Raman scattering

In this chapter, we shall illustrate the use of the scalar Wigner function approach (Sect. 2.2) on a typical laser–plasma interaction problem, namely the Stimulated Raman Scattering (SRS) [11–13, 41]. Our main purpose is to investigate the effect of the SRS on the spin dynamics in the case of a polarized electron plasma. A similar problem was studied recently using a hydrodynamic approach [42].

The SRS is a parametric instability, whereby an incident electromagnetic wave (ω_0,k_0) drives two waves inside the plasma: a scattered electromagnetic wave (ω_s,k_s) and an electron plasma wave (ω_e,k_e), where ω and k denote respectively the frequency and wave number of each wave. The plasma wave is responsible for the acceleration of the electron population, which is usually the intended purpose of the setup. Here, our objective is to investigate the effect of the electron spin on the SRS instability [43].

The waves must respect the following matching conditions (along their propagation direction, hereafter denoted x), which represent conservation of energy and momentum:

$$\omega_0=\omega_s+\omega_e,\quad k_0=k_s+k_e, \tag{10}$$

with dispersion relations: $\omega_{0,s}^2=\omega_p^2+c^2k_{0,s}^2$ and $\omega_e^2=\omega_p^2+3v_{th}^2k_e^2$, where $\omega_p=\sqrt{\frac{e\rho_0}{m\epsilon_0}}$ is the electron plasma frequency, $v_{th}=\sqrt{k_BT_e/m}$ is the thermal speed of an electron gas with temperature T_e, and k_B is the Boltzmann constant. Strictly speaking, the above dispersion relations are valid for an unpolarized electron plasma using Maxwell-Boltzmann statistics. The relevant dispersion relations for Fermi-Dirac statistics including spin effects are more involved and were derived recently in Ref. [44].

In order to obtain a tractable system of equations, we introduce some further assumptions that simplify the spin-Vlasov-Maxwell Eqs. (6)–(7). Following [41], we consider the case of a plasma that interacts with an electromagnetic wave propagating in the longitudinal x direction and assume that all fields depend on x only. Choosing the Coulomb gauge $\nabla\cdot\boldsymbol{A}=0$, the vector potential $\boldsymbol{A}$ lies in the perpendicular (transverse) plane $(y,\,z)$, i.e. $\boldsymbol{A}=(0,\boldsymbol{A}_\perp)$. Using $\boldsymbol{E}=-\nabla\phi-\partial_t\boldsymbol{A}$ and $\boldsymbol{B}=\nabla\times\boldsymbol{A}$, we get: $\boldsymbol{E}_\perp=-\partial_t\boldsymbol{A}_\perp$ and $E_x=-\partial_x\phi$, which imply that the electric field is mainly electromagnetic in the transverse plane and mainly electrostatic in the longitudinal direction.

We then consider a distribution function of the form: $g(\boldsymbol{r},\boldsymbol{v},\boldsymbol{s})\to\delta(m\boldsymbol{v}_\perp-e\boldsymbol{A}_\perp)g(x,v_x,\boldsymbol{s})$, which amounts to assuming that the plasma is cold in the transverse direction[1]. After integrating with respect to $\boldsymbol{v}_\perp$, the relevant extended phase space is reduced to 5D, i.e. position x, velocity v_x, and three components of the spin vector $\boldsymbol{s}$ (which can be reduced to two considering that the spin lies on the unit sphere).

A schematic view of this 1D configuration is shown on Fig. 1.

Finally, in the $(x,v_x,\boldsymbol{s})$ phase space, the scalar spin-Vlasov-Maxwell Eqs. (6)–(7) become:

[1] For a fully quantum plasma, described by a Fermi-Dirac distribution, the velocity dispersion does not vanish even at zero temperature, but would rather be determined by the Fermi velocity. In that case, the present transverse model should be modified.

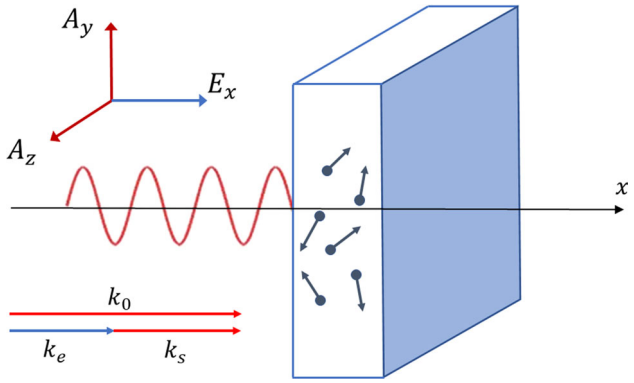

Fig. 1 Schematic view of our 1D configuration for SRS. All fields depend only on the longitudinal variable x. The electromagnetic wave is fully characterized by a transverse vector potential $\boldsymbol{A}_\perp = (A_y, A_z)$ and a longitudinal electrostatic field E_x. The wave vectors and frequency of the incident, scattered, and electromagnetic waves must obey the matching relations (10)

$$
\begin{aligned}
&\frac{\partial g}{\partial t} + v_x \frac{\partial g}{\partial x} + \left(E_x - H s_y \frac{\partial^2 A_z}{\partial x^2} + H s_z \frac{\partial^2 A_y}{\partial x^2} - \frac{1}{2} \frac{\partial |\boldsymbol{A}_\perp|^2}{\partial x} \right) \\
&\quad \frac{\partial g}{\partial v_x} + \boldsymbol{s} \times \boldsymbol{B} \cdot \frac{\partial g}{\partial \boldsymbol{s}} = 0, \\
&\frac{\partial E_y}{\partial t} = -\frac{\partial^2 A_y}{\partial x^2} + A_y \int g \, dv_x d\boldsymbol{s} + H \frac{\partial}{\partial x} \int s_z g dv_x d\boldsymbol{s}, \\
&\frac{\partial E_z}{\partial t} = -\frac{\partial^2 A_z}{\partial x^2} + A_z \int g \, dv_x d\boldsymbol{s} - H \frac{\partial}{\partial x} \int s_y g dv_x d\boldsymbol{s}, \\
&\frac{\partial E_x}{\partial x} = \int g \, dv_x d\boldsymbol{s} - 1,
\end{aligned}
\tag{11}
$$

where we have used nondimensional units, in which time is normalized to the inverse of the plasma frequency ω_p, space to the skin depth c/ω_p, velocities to c, densities to the uniform background ρ_0, and the scaled Planck constant is defined as $H = \hbar\omega_p/(2mc^2)$. The above spin-Vlasov-Maxwell system conserves the total energy, given by (in units of mc^2):

$$
\begin{aligned}
\mathcal{E} = &\underbrace{\frac{1}{2} \int v_x^2 g \, dx dv_x d\boldsymbol{s} + \frac{1}{2} \int |\boldsymbol{A}_\perp|^2 g \, dx dv_x d\boldsymbol{s}}_{\text{kinetic energy}} + \underbrace{\frac{1}{2} \int |\boldsymbol{E}|^2 dx}_{\text{electric energy}} \\
&+ \underbrace{\frac{1}{2} \int \left| \frac{\partial \boldsymbol{A}_\perp}{\partial x} \right|^2 dx}_{\text{magnetic energy}} + \underbrace{H \int \left(s_y \frac{\partial A_z}{\partial x} - s_z \frac{\partial A_y}{\partial x} \right) g dx dv_x d\boldsymbol{s}}_{\text{Zeeman energy}},
\end{aligned}
\tag{12}
$$

which is the sum of three components: kinetic, electromagnetic, and Zeeman energies.

Finally, we note that, although the standard spin-orbit coupling is absent from the above model (see Sect. (2.1)), there is still an interaction between the orbital and the spin degrees of freedom. This interaction is mediated by the self-consistent magnetic fields created by the electron currents, which in turn act on the electron spin. However, this effect requires large electronic currents that may be observed in dense plasmas, but usually not in condensed matter physics.

4 Simulation results

The Eq. (11) were solved numerically using a recently-developed PIC geometric scheme [43], with periodic boundaries in x with spatial period $L = 2\pi/k_e$. For the simulations shown here, we used $N_p = 2 \times 10^4$ particles and $N_x = 128$ grid points to solve the Maxwell equations. The time-step was $\Delta t = 0.04\,\omega_p$.

The initial condition is Maxwellian in velocity and uniform in space, with a small sinusoidal perturbation of amplitude α and wave number k_e:

$$
g(x, v_x, \boldsymbol{s}, t = 0) = \frac{1}{4\pi}(1 + \eta s_z)\,[1 + \alpha \cos(k_e x)]\, \frac{\exp(-v_x^2/2v_{th}^2)}{\sqrt{2\pi}\, v_{th}},
\tag{13}
$$

with $\alpha = 0.02$, $k_e = 1.22\,\omega_p/c$, and $v_{th} = 0.17c$ ($T_e = 15\,\text{keV}$) [41]. The constant $\eta \in [0, 1]$ represents the degree of spin polarization of the electrons, with $\eta = 1$ corresponding to a fully polarized gas. This is related to the average values of the spin components for our initial condition: $\langle s_x \rangle = \langle s_y \rangle = 0, \langle s_z \rangle = \eta/3$.

For the above temperature, the electron motion is borderline relativistic, so that in principle some relativistic corrections should be taken into account. For simplicity, here we do not consider these corrections (nor the spin-orbit coupling, which is also a relativistic effect, see Sect. 2.1). For a relativistic extension of the model without spin, see [41].

The initial transverse electromagnetic field is taken to be a circularly polarized wave with wave vector (along x) $k_0 = 2k_e$ and electric field amplitude $E_{\perp,0} \equiv E_0 = 0.325\, mc\omega_p/e$. We expect that a circularly polarized wave will be more efficient in coupling to the spin degrees of freedom of the electron gas. The matching conditions (10) then yield: $k_s = k_e$, $\omega_0 = 2.63\,\omega_p$, $\omega_s = 1.56\,\omega_p$, and $\omega_e = 1.06\,\omega_p$. Further, we take $\eta = 1$ and $H = 2.3 \times 10^{-4}$, which correspond to a fully polarized electron gas with average density $\rho_0 = 4 \times 10^{31}\,\text{electrons/m}^3$.

Figure 2 (left frame) shows the longitudinal electric energy $\frac{\epsilon_0}{2} \int E_x^2 dx$ as a function of time (this is actually an energy per unit surface, since the plasma is infinite in the transverse plane). It is initially very small, as it represents the internal electrostatic energy of the plasma, which vanishes for a homogeneous equilibrium, i.e., when $\alpha = 0$ in Eq. (13). The early exponential growth represents the onset of the parametric Raman

instability. The instability rate observed in the simulation is close to the one predicted by the theory in the absence of spin effects, $\gamma \approx 0.04\,\omega_p$ [41]. After saturation of the instability, one enters the nonlinear regime, in which the electrostatic energy settles on an approximately constant value significantly smaller than the peak attained at the end of the linear regime. (We note that, given the physical regime studied here, the effect of the spin on the onset of the instability is rather small. However, the main purpose of this work is to estimate the loss of polarization and coherence of the initially polarized electron gas following the SRS instability, as will be apparent from the forthcoming results).

In contrast, the magnetic energy per unit surface $\frac{1}{2\mu_0}\int |\boldsymbol{B}_\perp|^2 dx$ is transverse and is carried by the electromagnetic wave. Its initial amplitude is proportional to the square of the wave amplitude $E_{\perp,0}$ and therefore considerably higher than the initial electrostatic energy. During the same period of time (Fig. 2, right frame), this term decreases by a factor ≈ 4.5, signalling that the energy of the electromagnetic wave is greatly absorbed by the plasma, and transformed partly into electrostatic energy (left frame of Fig. 2) and partly into kinetic energy, i.e., heating.

We note that our PIC code conserves the total energy, as given by Eq. 12, with very good accuracy: $\delta\mathcal{E}/\mathcal{E} < 5\times 10^{-4}$.

The y and z components of the average spin vector (Fig. 3) display some oscillations at the low frequency $\omega_{\rm spin} \approx 0.01\,\omega_p$, which are progressively damped away (the x component is very small and remains such during the entire run). It can be shown [43] that, in the regime where the Larmor frequency $\omega_L = eB_0/m$ (where $B_0 = k_0 E_0/\omega_0$ is the magnetic field of the incident wave) is much smaller than the frequency ω_0 of the wave itself, the spin component $S_z(t)$ rotates with a frequency $\omega_{\rm spin} = \omega_L^2/(2\omega_0)$. With our parameters, this yields $\omega_{\rm spin} = 0.0176\,\omega_p$, which is not far from the value observed in Fig. 3, considering that this simple analytical estimate neglects all effects due to the Raman instability and self-consistent fields.

Another interesting quantity to investigate is the *quantum purity* of the system. In the present case, which is partly classical (for the orbital variables) and partly quantum (for the spin), it is not possible to define a global density matrix. However, we can define a reduced density matrix for the spin degrees of freedom.

To do so, we make use of the definition of g, Eq. (9), to write: $f_0 = \int g ds$ and $\boldsymbol{f} = 3\int \boldsymbol{s} g ds$, and then obtain the 2×2 Wigner function $\mathcal{F}$ through Eq. (2). The reduced density matrix $\hat{\rho}$ is computed by integrating over the phase-space variables:

$$\hat{\rho} = \int\int \mathcal{F}(x, v_x)\, dx dv_x = \frac{1}{2}(\mathbb{I} + 3\,\boldsymbol{\sigma}\cdot\langle \boldsymbol{s}\rangle), \quad (14)$$

where $\mathbb{I}$ is the identity matrix. Finally, we can compute the purity:

$$P(t) \equiv {\rm Tr}\hat{\rho}^2 = \frac{1 + 9\,|\langle \boldsymbol{s}\rangle|^2}{2}. \quad (15)$$

Note that, at $t = 0$, $\langle s_x\rangle = \langle s_y\rangle = 0, \langle s_z\rangle = \eta/3$, hence $P(0) = (1+\eta^2)/2$. In the case studied here $\eta = 1$, so that $P(0) = 1$, i.e. the initial state is a pure one. More generally, the initial density matrix can be written as:

$$\hat{\rho}_{t=0} = \frac{1}{2}\begin{pmatrix} 1+\eta & 0 \\ 0 & 1-\eta \end{pmatrix}. \quad (16)$$

For a completely unpolarized gas $\eta = 0$ and the density matrix is that of a maximally mixed state.

The time evolution of the quantum purity is shown in Fig. 4 and begins at $P(0) = 1$ (apart from sampling errors due to the finite number of particles in the PIC code). As the spin system is not isolated, but rather interacts with the (classical) orbital degrees of freedom, there is no reason why the purity of the reduced spin density matrix should stay constant. This is what we observe in our simulation.

Two points are noteworthy. First, the behaviour of the purity is not monotonous: it decreases initially until $\omega_p t \approx 300$, then grows until $\omega_p t \approx 1000$, after which it again decreases monotonically. The lapse of time where the purity grows appears to correspond to the change in behaviour of the electric and magnetic energies observed in Fig. 2, as if the system tried to settle down at an equilibrium with higher electromagnetic energies, but finally relaxes to a lower energy state.

Second, the purity appears to reach asymptotically the value: $P(t\to\infty) = 0.5$, which is the purity of a maximally mixed system, with vanishing polarization ($\eta = 0$). Thus, after around $3000\,\omega_p^{-1}$ the initial spin polarization has been entirely lost. With our chosen parameters, this corresponds to approximately 8.4 fs.

5 Conclusions

The primary aim of this work was to illustrate how quantum effects (particularly the electron spin) can impact ultrafast laser-matter interactions. To this purpose, we proposed to use a phase-space approach, based on Wigner functions, which includes the spin degrees of freedom. In this hybrid model, the orbital electronic motion is treated classically, while the spin is considered as a fully quantum variable. The resulting spin-Vlasov equation can be coupled to the full Maxwell equations to obtain a self-consistent mean-field model.

In practice, the spin-Vlasov equations can be written in two equivalent forms: (i) a scalar form, where the probability distribution is defined over an extended phase space that includes not only position and momentum, but also a spin variable, and (ii) a matrix form, where the probability distribution is a 2×2 matrix that depends only on the standard phase-space variables.

Here, we used the scalar approach to investigate the effect of the electron spin on the stimulated Raman scattering, a well-known effect in laser–plasma physics. An efficient PIC code, based on a geometric Hamiltonian technique, was developed recently to solve the

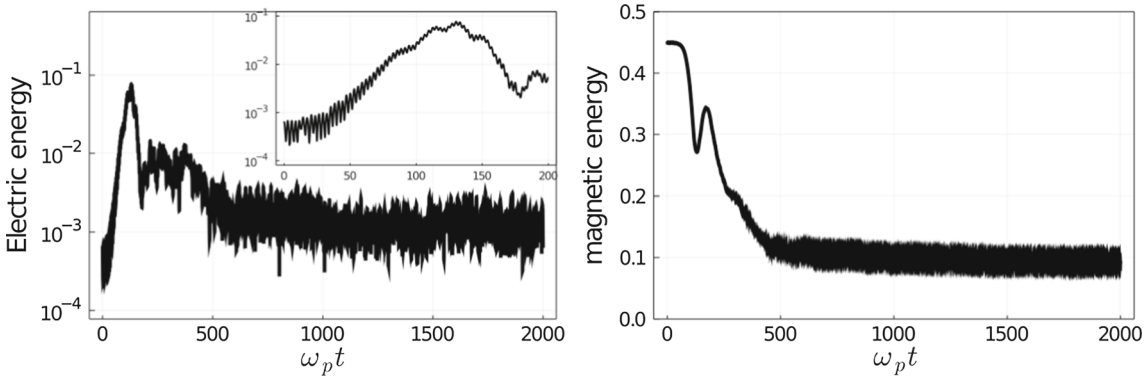

Fig. 2 Electrostatic energy $\frac{\epsilon_0}{2}\int E_x^2 dx$ (left frame) and magnetic energy $\frac{1}{2\mu_0}\int |\boldsymbol{B}_\perp|^2 dx$ (right frame) as a function of time. The inset shows a zoom of the electrostatic energies at short times, evidencing the exponential growth of the Raman instability. Both energies are expressed in units of mc^2

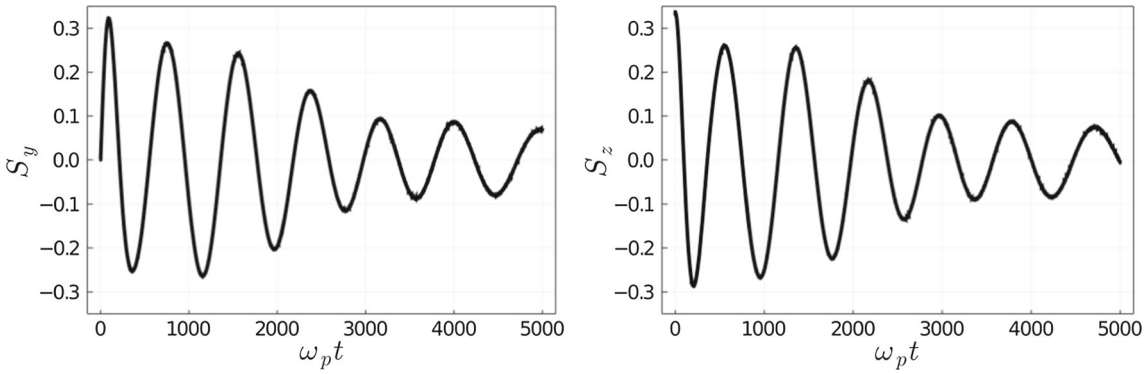

Fig. 3 Time evolution of the components of the average spin vectors: $S_y(t) = \langle s_y \rangle$ (left frame) and $S_z(t) = \langle s_z \rangle$ (right frame). The x component remains very small all along the duration of the run

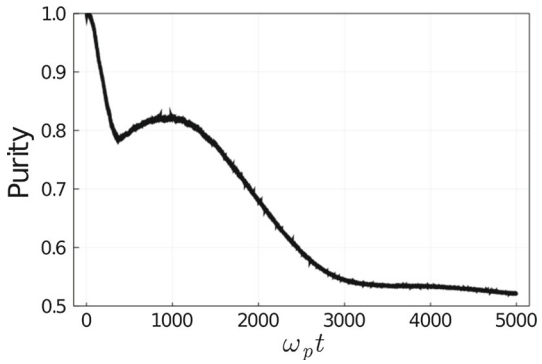

Fig. 4 Time evolution of the spin purity

spin-Vlasov-Maxwell equations [43]. The simulations indicate that, following the Raman parametric instability, an initially spin-polarized plasma loses its magnetization in about 500 plasma periods. The polarization is related to the purity of the reduced spin density matrix (obtained by tracing over the orbital degrees of freedom). We observed that the spin system, which is initially in a pure quantum state corresponding to spin-up in the z direction, turns into a maximally mixed state (50/50 mixture of spin-up and spin-down states) over the same lapse of time.

Future work will involve the implementation of a grid-based method to solve the spin-Vlasov-Maxwell equations in the matrix formalism of Sect. 2.1. The matrix approach was already used to study the generation of spin currents in nickel films [36]. The next step will be the development of an accurate grid-based code that uses the same geometric Hamiltonian approach as the PIC code employed in the present work.

References

1. C. Voisin, D. Christofilos, N. Del Fatti, F. Vallée, B. Prével, E. Cottancin, J. Lermé, M. Pellarin, M. Broyer, Phys. Rev. Lett. **85**, 2200 (2000). https://doi.org/10.1103/PhysRevLett.85.2200. (**ISSN 0031-9007**)
2. J.-Y. Bigot, V. Halté, J.-C. Merle, A. Daunois, Chem. Phys. **251**, 181 (2000)
3. O. Salata, J. Nanobiotechnol. **2**, 3 (2004), ISSN 1477-3155, http://www.ncbi.nlm.nih.gov/pubmed/15119954
4. L. Loomba, T. Scarabelli, Therapeutic Delivery **4**, 1179 (2013), ISSN 2041-5990, http://www.ncbi.nlm.nih.gov/pubmed/24024515https://doi.org/10.4155/tde.13.74

5. J. Butet, J. Duboisset, G. Bachelier, I. Russier-Antoine, E. Benichou, C. Jonin, P.-F. Brevet, Nano Lett. **10**, 1717 (2010). https://doi.org/10.1021/nl1000949
6. H. Singhal, R. A. Ganeev, P. A. Naik, A. K. Srivastava, A. Singh, R. Chari, R. A. Khan, J. A. Chakera, P. D. Gupta, J. Phys. B: Atom. Mol. Opt. Phys. **43**, 025603 (2010), ISSN 0953-4075, http://stacks.iop.org/0953-4075/43/i=2/a=025603?key=crossref.49a4d77b18731634172632dc777fb0db
7. J. Hurst, O. Morandi, G. Manfredi, P.-A. Hervieux, Eur. Phys. J. D **68**, 176 (2014). arXiv:1405.1184
8. V.T. Tikhonchuk, Philos. Trans. R. Soc. A: Math. Phys. Eng. Sci. **378**, 20200013 (2020). https://doi.org/10.1098/rsta.2020.0013
9. V. Malka, Phys. Plasmas **19**, 055501 (2012). https://doi.org/10.1063/1.3695389
10. T. Tajima, V. Malka, Plasma Phys. Controlled Fusion **62**, 034004 (2020). https://doi.org/10.1088/1361-6587/ab6da4
11. D. Forslund, J. Kindel, E. Lindman, Phys. Fluid **18**, 1002 (1975)
12. C.J. Walsh, D.M. Villeneuve, H.A. Baldis, Phys. Rev. Lett. **53**, 1445 (1984). https://doi.org/10.1103/PhysRevLett.53.1445
13. A. Modena, Z. Najmudin, A. Dangor, C. Clayton, K. Marsh, C. Joshi, V. Malka, C. Darrow, C. Danson, D. Neely et al., Nature **377**, 606 (1995)
14. A. Alekhin, I. Razdolski, N. Ilin, J.P. Meyburg, D. Diesing, V. Roddatis, I. Rungger, M. Stamenova, S. Sanvito, U. Bovensiepen et al., Phys. Rev. Lett. **119**, 017202 (2017)
15. A. Hirohata, K. Yamada, Y. Nakatani, I.-L. Prejbeanu, B. Diény, P. Pirro, B. Hillebrands, J. Magn. Magn. Mater. **509**, 166711 (2020)
16. E. Beaurepaire, J.-C. Merle, A. Daunois, J.-Y. Bigot, Phys. Rev. Lett. **76**, 4250 (1996). https://doi.org/10.1103/PhysRevLett.76.4250
17. K. Krieger, J. Dewhurst, P. Elliott, S. Sharma, E. Gross, J. Chem. Theory Comput. **11**, 4870 (2015)
18. M. Stamenova, J. Simoni, S. Sanvito, Phys. Rev. B **94**, 014423 (2016). https://doi.org/10.1103/PhysRevB.94.014423
19. M. Battiato, K. Carva, P.M. Oppeneer, Phys. Rev. Lett. **105**, 027203 (2010). https://doi.org/10.1103/PhysRevLett.105.027203. (**ISSN 0031-9007**)
20. Y. Wu, L. Ji, X. Geng, Q. Yu, N. Wang, B. Feng, Z. Guo, W. Wang, C. Qin, X. Yan et al., New J. Phys. **11**, 073052 (2019)
21. Y. Wu, L. Ji, X. Geng, J. Thomas, M. Büscher, A. Pukhov, A. Hützen, L. Zhang, B. Shen, R. Li, Phys. Rev. Appl. **13**, 044064 (2020)
22. Z. Nie, F. Li, F. Morales, S. Patchkovskii, O. Smirnova, W. An, N. Nambu, D. Matteo, K.A. Marsh, F. Tsung et al., Phys. Rev. Lett. **126**, 054801 (2021)
23. S.C. Cowley, R.M. Kulsrud, E. Valeo, Phys. Fluids **29**, 430 (1986)
24. J. Hurst, P.-A. Hervieux, G. Manfredi, Philos. Trans. R. Soc. A: Math. Phys. Eng. Sci. **375**, 20160199 (2017). https://doi.org/10.1098/rsta.2016.0199
25. J. Zamanian, M. Marklund, G. Brodin, New J. Phys. **12**, 043019 (2010a), http://stacks.iop.org/1367-2630/12/i=4/a=043019?key=crossref.153368f55cfe1c0f5f8e618f46552dfd
26. J. Zamanian, M. Stefan, M. Marklund, G. Brodin, Phys. Plasmas **17**, 102109 (2010b), http://scitation.aip.org/content/aip/journal/pop/17/10/10.1063/1.3496053
27. O. Morandi, J. Zamanian, G. Manfredi, P.-A. Hervieux, Phys. Rev. E **90**, 013103 (2014), https://doi.org/10.1103/PhysRevE.90.013103
28. G. Brodin, A. Holkundkar, M. Marklund, J. Plasma Phys. **79**, 377 (2013)
29. F. Li, V.K. Decyk, K.G. Miller, A. Tableman, F.S. Tsung, M. Vranic, R.A. Fonseca, W.B. Mori, J. Comput. Phys. **438**, 110367 (2021). (**ISSN 0021-9991**)
30. R. Sinha-Roy, J. Hurst, G. Manfredi, P.-A. Hervieux, ACS Photonics **7**, 2429 (2020). https://doi.org/10.1021/acsphotonics.0c00462
31. Y. Yin, P.-A. Hervieux, R.A. Jalabert, G. Manfredi, E. Maurat, D. Weinmann, Phys. Rev. B **80**, 115416 (2009). https://doi.org/10.1103/PhysRevB.80.115416. (**ISSN 1098-0121**)
32. G. Manfredi, P.-A. Hervieux, Y. Yin, N. Crouseilles, *Collective Electron Dynamics in Metallic and Semiconductor Nanostructures* (Springer Berlin Heidelberg, Berlin, Heidelberg, 2010), pp. 1–44, ISBN 978-3-642-04650-6, https://doi.org/10.1007/978-3-642-04650-6_1
33. G. Manfredi, P.-A. Hervieux, J. Hurst, Rev. Modern Plasma Phys. **3**, 1 (2019)
34. A. Arnold, H. Steinrück, ZAMP Zeitschrift für angewandte Mathematik und Physik **40**, 793 (1989). https://doi.org/10.1007/BF00945803
35. O. Morandi, F. Schürrer, J. Phys. A: Math. Theor. **44**, 265301 (2011), http://stacks.iop.org/1751-8121/44/i=26/a=265301?key=crossref.9c38a6baa4753b3171f66c02867efa02
36. J. Hurst, P.-A. Hervieux, G. Manfredi, Phys. Rev. B **97**, 014424 (2018). https://doi.org/10.1103/PhysRevB.97.014424
37. M. Marklund, J. Zamanian, G. Brodin, Transport Theory Stat. Phys. **39**, 502 (2010). https://doi.org/10.1080/00411450.2011.566502
38. G. Brodin, M. Marklund, J. Zamanian, M. Stefan, Plasma Physics and Controlled Fusion **53**, 074013 (2011), http://stacks.iop.org/0741-3335/53/i=7/a=074013?key=crossref.6598251ca96ba298ee582aad4c09a7ec
39. G. Brodin, M. Marklund, J. Zamanian, S. Ericsson, P.L. Mana, Phys. Rev. Lett. **101**, 245002 (2008)
40. P.A. Andreev, L.S. Kuz'menkov, Phys. Plasmas **24**, 112108 (2017). https://doi.org/10.1063/1.4999103
41. A. Ghizzo, P. Bertrand, M. Shoucri, T. Johnston, E. Fijalkow, M. Feix, J. Comput. Phys. **90**, 431 (1990)
42. M. Shahid, Z. Iqbal, M. Jamil, G. Murtaza, Phys. Plasmas **24**, 102113 (2017). https://doi.org/10.1063/1.4986010
43. N. Crouseilles, P.-A. Hervieux, Y. Li, G. Manfredi, Y. Sun, J. Plasma Phys. **87**, 825870301 (2021)
44. G. Manfredi, P.-A. Hervieux, J. Hurst, Rev. Modern Plasma Phys. **5**, 1 (2021)